Microfibrils provide non-linear elastic behaviour in the abdominal artery of the lobster *Homarus americanus*

Colin J. McConnell, M. Edwin DeMont* and Glenda M. Wright†

Biology Department, PO Box 5000, St Francis Xavier University, Antigonish, Nova Scotia, Canada B2G 2W5 and †Department of Anatomy and Physiology, Atlantic Veterinary College, University of Prince Edward Island, Charlottetown, Prince Edward Island, Canada C1A 4P3

1. Microfibrils are becoming increasingly recognized as an important component of the extracellular matrix. However, almost nothing is known about their mechanical role in the diversity of tissues in which they are found.

2. Microfibrils form the principal structural component in the wall of the abdominal artery of the lobster *Homarus americanus*. We have used previous estimates of the mechanical properties of these microfibrils, estimates of the fraction of the aorta wall volume occupied by the microfibrils, and their angular distribution as a function of strain in a numerical model that predicts the macroscopic mechanical properties of the whole tissue.

3. Microfibrils alone, when their reorientation and deformation are accounted for, characterize the stress–strain behaviour of the vessel. Evidence of the evolutionary conservation of fibrillin between medusans, echinoderms and vertebrates implies that the mechanical properties of lobster microfibrils may apply to microfibrillar function in other taxa. This will have profound implications on the perceived roles of microfibrils in development, physiology and disease.

Microfibrils form a proteinaceous component of the extracellular matrix found in a variety of tissues in many animals. Most research into microfibrils to date has concentrated on their identification, description of their ultrastructure (Keene, Maddox, Kuo, Sakai & Granville, 1991; Kielty, Cummings, Whittaker, Shuttleworth & Grant, 1991) and determination of their chemistry (Sakai, Keene & Engville, 1986). The principal protein in vertebrate microfibrils is fibrillin, and recently the organization of fibrillin in the microfibrils has been examined (Reinhardt *et al.* 1996). The functional role played by microfibrils is not understood and may vary depending on the developmental stage of the tissue in which they are found.

The morphology of elastic tissue containing microfibrils was recently reviewed (Montes, 1992). Groups of bundles of mammalian microfibrils are known as oxytalan fibres. The ciliary zonules in mature mammals are composed solely of oxytalan fibres. A fibre that is composed of both elastin and microfibrils is termed an elaunin fibre. One that is chiefly elastin, with only a microfibrillar boundary is called an elastic fibre. During development, amorphous elastin is deposited on the microfibrillar scaffolding. Thus, the mature elastic fibres develop within a framework of microfibrils that must function as a complete elastic element before the elastin becomes functional (Mecham & Heuser, 1991; Montes, 1992; Malak & Bell, 1994).

Marfan syndrome (MFS), an important human hereditary disease of the connective tissues, is characterized by irregularities in the synthesis of the protein fibrillin, an essential part of vertebrate microfibrils (Godfrey, Menache & Weleber, 1990; Ramirez, Pereira, Zhang & Lee, 1993; Hollister, Godfrey & Sakai, 1994; Godfrey, Michael & Steinmann, 1995). One of the things that makes MFS so intriguing to researchers is the fact that the profound loss of function is completely out of proportion to the relatively small bulk of affected tissue. Clearly the mechanical role played by these microfibrils bears closer examination. This study will be important for biomedical research because little is known of microfibrillar function generally.

Microfibrils are also found in invertebrate tissues. Recently, a homology has been reported (Reber-Müller, Spissinger, Schuchert, Spring & Schmid, 1995) between an extracellular matrix protein of the jellyfish *Podocoryne carnea* and mammalian fibrillins. The protein is observed to form fibrillin-like beaded microfibrils, and a cDNA fragment of the gene coding for this protein shows a >40% identity in sequences to human fibrillin genes. Mechanical studies have been performed (DeMont & Gosline, 1988) on the radial elastic fibres in the mesoglea of another jellyfish, *Polyorchis penicillatus* and from the descriptions of DeMont & Gosline, (1988) and Reber-Müller *et al.* (1995) it seems clear that they examined the same tissues. DeMont & Gosline (1988)

* To whom correspondence should be addressed.

examined the energetics of locomotion and were able to predict the modulus of elasticity of the radial elastic fibres, which was 1·0 MPa. Thurmond (1996) performed mechanical and biochemical analyses of microfibrils in the dermis of the sea cucumber *Cucumaria frondosa*. He reported a modulus of elasticity of 0·2 MPa, and his measurements were based on an extrapolation from the macroscopic properties of the sea cucumber dermis.

Microfibrils are the principal structural component of arteries found in primitive vertebrates and invertebrates (Davison, Wright, & DeMont, 1995). McConnell *et al.* (1996) used these microfibrillar-based primitive arteries to measure the mechanical properties of individual microfibrils. The calculated modulus of elastcity of 1·06 MPa for microfibrils in the abdominal aorta of the lobster is very close to the modulus of elastin, which is 1·2 MPa (Aaron & Gosline, 1981). Since microfibrils in mammals have been previously thought to function solely as extracellular 'scaffolding' on which elastin is deposited in the development of elaunin fibres (Montes, 1992), this is an intuitively reasonable result. Because cnidarians and sea cucumbers (echinoderms) are thought to have evolved before both vertebrates and crustaceans, it is reasonable to speculate that there is a homology between lobster and mammalian microfibrils. The observed linear deformation behaviour and modulus of elasticity of lobster artery microfibrils imply that mammalian microfibrils may similarly have a mechanical function as well as the established developmental role as 'depositional scaffolding' (Montes, 1992).

A comparative study of the structure and mechanical properties of these microfibril-based arteries has been completed (Davison *et al.* 1995). It showed that the arteries exhibit non-linear elastic behaviour, typical of other vertebrate (Shadwick, 1992) and invertebrate arteries (Shadwick & Gosline, 1985) that have been studied previously. The non-linearity is functionally important, for reasons that have been described previously (Shadwick, 1992). For vertebrate arteries, the non-linearity has been attributed to deformation of the elastin component at low strains and collagen at high strains. In this paper we develop a mathematical model of the mechanical behaviour of the arteries of the lobster *Homarus americanus* and show that the non-linearity can be attributed to reorientation of the microfibrils at the low end of the stress–strain curve and to deformation of the microfibrils themselves at the high end of the stress–strain curve.

The model

A variety of mathematical models have been published in order to promote an understanding of fibrous composite biomaterials in general, and arteries in particular (Bergel, 1961; Hudetz, 1979; Aspden, 1986; Ault & Hoffman, 1992*a*, *b*). One of the complications, and great challenges, has been partitioning the stress–strain curve to account for reorientation of reinforcing fibres, as well as their deformation.

Ault & Hoffman (1992*a*, *b*) detail a model that takes into account fibre reorientation, as well as fibre–matrix interaction. The model is comprehensive, but some of its parameters (e.g. elastic modulus and Poisson's ratio of the matrix) are difficult to determine experimentally. The model outputs delimit upper and lower bounds which enclose the true material behaviour. Other methods (Bergel, 1961; Hudetz, 1979) produced formulations that explain observed data, but are not very predictive. Aspden's (1986) approach deals primarily with fibre reorientation within the material. The model assumes that the fibres are nominally infinitely long and that the transfer length is relatively short in comparison with the length of the fibres, and thus the fibres are fully load bearing. With this assumption, the model is capable of predicting longitudinal stress in a material, given the orthogonal strains. We will not attempt to reproduce the full derivation here; the interested reader is directed to the original citation. However, the details of the model development for this case may be instructive, and are included in Appendix 1.

The model is based primarily on the definition of Young's modulus (E). This quantity is the slope of the line of a plot of stress (σ) against strain (ϵ). Algebraically, then, E is the ratio of σ and ϵ. Since strain is the experimentally measured variable, and the modulus is calculated from the measured strain, the stress is calculable from:

$$\sigma = E\epsilon. \tag{1}$$

This relation holds only for solid materials. In lobster arterial wall, the volume is not occupied solely by microfibrils, so the contributions made by the microfibrils and cellular matrix must be accounted for separately:

$$\sigma = E_{\mathrm{f}} V_{\mathrm{f}} \epsilon_{\mathrm{f}} + E_{\mathrm{m}}(1 - V_{\mathrm{f}})\epsilon_{\mathrm{m}}, \tag{2}$$

where V denotes volume fraction, and variables subscripted f are properties of the fibres, while those subscripted m are properties of the matrix. It is explicitly assumed that the reinforcing fibres are stiff in tension, but compliant in compression due to buckling, and that the opposite is true of the matrix. Applying this assumption to the geometry of the lobster artery leads to the inference that the matrix plays no role in carrying circumferential loads, and the microfibrils carry none of the radial load. Note that only the two-dimensional case need be considered. Thus, for this case, the contribution of the matrix may be neglected and eqn (2) rewritten as:

$$\sigma = E_{\mathrm{f}} V_{\mathrm{f}} \epsilon_{\mathrm{f}}. \tag{2a}$$

The innovation in Aspden's (1986) model lies in accounting for the orientation of the reinforcing fibres with respect to the direction of the applied load. The orientation of a single fibre is treated as a random variable, described by a distribution function, $g(\theta)$. The actual fibre reorientation is not treated in the conventional trigonometric fashion. Instead of multiplying the fibre length by the cosine of the angle that the fibre's new direction makes with the old

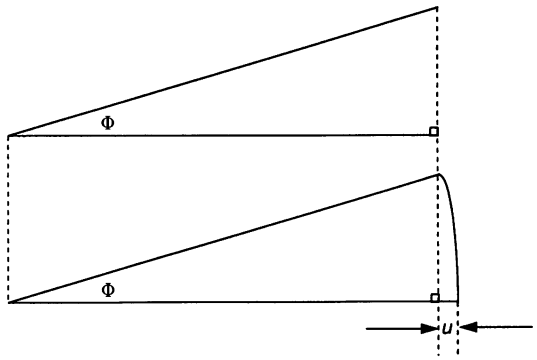

Figure 1. Fibre reorientation is better accomplished through the use of direction cosines than conventional trigonometry
Through an angular change of Φ deg, trigonometry underestimates the length of the fibre in the new direction by an amount u, while the use of direction cosines preserves the original length and changes only the fibre direction.

direction (θ), the change in direction is treated with the more rigorous application of direction cosines. Simply multiplying the fibre length by the cosine of θ treats the original fibre length as the hypotenuse of a right triangle, and so the fibre length in the new direction is shorter than the original. A more realistic image of the reorientation, rather than two sides of a triangle, is two radii of a circle (Fig. 1). Using direction cosines to calculate reorientation allows the fibre to be treated as if it were sweeping out an arc of a circle. The reorientation does not affect the length of the fibre, only its position in space. So, accounting for the reorientation of a single fibre, without loss of generality:

$$\sigma_{ij} = V_f E_f \epsilon_f \theta l'_i l'_j, \tag{3}$$

where l'_i and l'_j are direction cosines and the subscripts i and j denote summation over repeated indices. In a many fibre system, θ is replaced by an angular distribution function, $g(\theta)$, and the reorientation must be integrated over the range of angles included in $g(\theta)$ for each increment in strain. Thus:

$$\Delta\sigma_{ij} = \int_{-\pi/2}^{\pi/2} V_f E_f \Delta\epsilon_f g(\theta) l'_i l'_j \mathrm{d}\theta. \tag{4}$$

This, then, is the essence of Aspden's (1986) model. Each of the factors influencing the fibre behaviour is given equal multiplicative weight.

The fibres are assumed to be normally distributed about a perpendicular to a radial line cutting through the vessel wall. The distribution may then be calculated, based on the standard deviation of the observed angular distribution from experimental samples, as:

$$g(\theta) = \frac{1}{S(\epsilon)\sqrt{2\pi}} \exp\{[-(\theta - \bar{\theta})^2]/[2S^2(\epsilon)]\}, \tag{5}$$

where $S(\epsilon)$ is the standard deviation of angles as a function of strain, and $\bar{\theta}$ is the mean angle of the function.

Substituting eqn (5) into eqn (4), and bringing all factors with no dependence on θ outside the integral leaves:

$$\Delta\sigma_{ij} = \frac{V_f E_f}{S(\epsilon)\sqrt{2\pi}} \int_0^{\pi} \Delta\epsilon_f \exp\{[-(\theta_i - \bar{\theta})^2]/[2S^2(\epsilon)]\} l'_i l'_j \mathrm{d}\theta. \tag{6}$$

This equation, while concise, is not in an easily computable form. First of all, the limits of integration are artificially wide. There is no need to integrate over an entire semicircle, since most of the fibres will not be sufficiently aligned with the tension vector to contribute in supporting the imposed stress over much of the loading curve. Only those fibres in the range $0 \leqslant \theta \leqslant \theta_{max}$ need be considered, where:

$$\theta_{max} = \cos^{-1} \sqrt{\frac{1 - (1 + \epsilon_r)^2}{(1 + \epsilon_c)^2 - (1 + \epsilon_r)^2}}, \tag{7}$$

where subscripts r and c denote radial and circumferential quantities, respectively. Furthermore, eqn (6) represents not one but four integrals, since the two dimensional stress is a tensor. However, both of the off-diagonals are zero, and it is explicitly assumed that the microfibrils are weak in

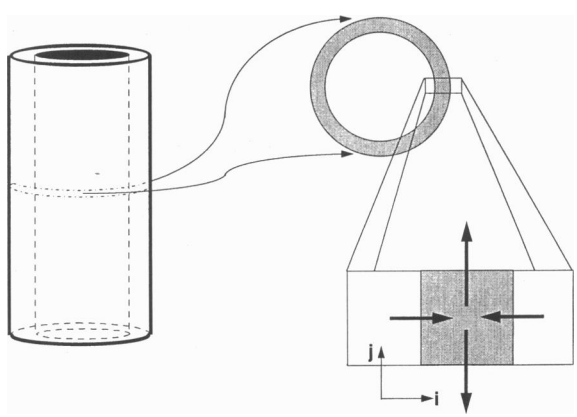

Figure 2. Schematic of an artery under pressure
Internal pressure vector is balanced by an external reaction vector (the i direction), putting the vessel in compression radially. Only tension vectors act in the direction of component microfibrils (the j direction).

$$\Delta\sigma_{22} = \frac{V_f E_f}{S(\epsilon)\sqrt{2\pi}}\left(\int_0^{\theta_{max}} \frac{\epsilon_1(1+\epsilon_1)(1+\epsilon_2)^2\sin^2\theta\cos^2\theta\exp\{[-(\theta_i-\bar{\theta})^2]/[2S^2(\epsilon)]\}}{[(1+\epsilon_1)^2\cos^2\theta+(1+\epsilon_2)^2\sin^2\theta]^{3/2}}d\theta\right.$$

$$+\int_0^{\theta_{max}} \frac{\epsilon_2(1+\epsilon_2)^3\sin^4\theta\exp\{[-(\theta_i-\bar{\theta})^2]/[2S^2(\epsilon)]\}}{[(1+\epsilon_1)^2\cos^2\theta+(1+\epsilon_2)^2\sin^2\theta]^{3/2}}d\theta$$

$$+\int_0^{\theta_{max}} \frac{(1+\epsilon_1)(1+\epsilon_2)^2\sin^2\theta\cos^2\theta\exp\{[-(\theta_i-\bar{\theta})^2]/[2S^2(\epsilon)]\}}{[(1+\epsilon_1)^2\cos^2\theta+(1+\epsilon_2)^2\sin^2\theta]^{3/2}}d\theta$$

$$+\int_0^{\theta_{max}} \frac{(1+\epsilon_2)^3\sin^4\theta\exp\{[-(\theta_i-\bar{\theta})^2]/[2S^2(\epsilon)]\}}{[(1+\epsilon_1)^2\cos^2\theta+(1+\epsilon_2)^2\sin^2\theta]^{3/2}}d\theta$$

$$\left.+\int_0^{\theta_{max}} \frac{(1+\epsilon_2)^2\sin^2\theta\exp\{[-(\theta_i-\bar{\theta})^2]/[2S^2(\epsilon)]\}}{(1+\epsilon_1)^2\cos^2\theta+(1+\epsilon_2)^2\sin^2\theta}d\theta\right).$$

Equation 8

compression, so they play no role in supporting circumferential stress. That leaves only one integral shown in expanded form in eqn (8). The subscripts 1 and 2 refer to radial and circumferential quantities, respectively, in the co-ordinate system defined in Fig. 2. The 'strains' in this equation are not true strains, however, but strain increments, so:

$$\epsilon_1 = \epsilon_{i(n)} - \epsilon_{i(n-1)},$$

and:

$$\epsilon_2 = \epsilon_{j(n)} - \epsilon_{j(n-1)}.$$

The model provides a means of accounting for any strain already present when each new increment of strain is calculated. This feature is essential for any material whose constituents display non-linear elastic behaviour, since the modulus of elasticity will change with changes in strain. Since the microfibrils display linear deformation behaviour, each strain increment produces the same amount of deformation in a single fibril as the last, or the next. Therefore, it is not necessary in this case to account for this 'memory of deformation'. In spite of the seeming complexity of eqn (8), all inputs are experimentally determinable. McConnell, Wright & DeMont (1996) measured E_f and Davison *et al.* (1995) described a means of determining ϵ_1 and ϵ_2. The only parameters yet to be determined are V_f and $S(\epsilon)$, and the method follows.

METHODS

Data collection

Specimens of the lobster *Homarus americanus* were purchased locally. All animals were maintained and killed according to the guidelines set by the Canadian Council of Animal Care. Animals were killed by bubbling CO_2 into a container of seawater for 20 min. Abdominal arteries were removed and fixed as described in previous work (McConnell *et al.* 1996).

The glutaraldehyde-only fixed vessels were postfixed for 1 h in 1 % OsO_4 in seawater at room temperature. All tissues were then dehydrated in ethanol through propylene oxide and embedded in epon–araldite. One micrometre thick transverse sections were mounted on glass slides and stained with Toluidine Blue. Ultrathin sections (70 nm thick) were collected on 200 mesh copper grids and stained with uranyl acetate and lead stain. The inner circumference and wall thickness were measured from the Toluidine Blue sections. Three micrographs were taken adjacent to the lumen of each pressurized section, and four random probe micrographs taken from each zero-stress sample. The micrographs were taken using a Hitachi H600 electron microscope, operating at 75 kV. The final magnification of the micrographs was ×95 000. Micrographs were analysed with Bioquant for OS2, version 2.6 (R&M Biometrics Inc., Nashville, TN, USA). This software was used to digitize the micrographs and to make all measurements.

The microfibrils are not distributed uniformly across the wall of the vessel, but are aggregated into fibre bundles, which are distributed evenly across the vessel wall. To measure the volume fraction of microfibrils in a fibre bundle (V_F), a variation on the point counting method was used (Weibel, 1979). A line was marked on a digital image of a micrograph, and the proportion of its length covered by the microfibrils was determined. This procedure was followed four

times per micrograph. To determine the volume fraction of fibre bundles in the vessel wall (V_b), a similar procedure was carried out on Toluidine Blue stained thick sections of OsO_4 fixed vessels. A radial line through the wall was measured, and the proportion of that line covered by fibre bundles was determined. This was repeated ten times for each thick section. The product of these two ratios was used as the volume fraction of microfibrils (V_f).

The model parameter $S(\epsilon)$ requires a knowledge of both the standard deviations of the distribution of angles that the microfibrils form with a radial line and the strains in the vessel wall which correspond to those distributions.

The standard deviations of angular distributions were determined from the same micrographs used in previous work (McConnell *et al.* 1996). The utility for measuring angles incorporated within the Bioquant package links this measurement to the longest linear dimension of a measured area. The system measures all angles with respect to a horizontal line parallel to the image monitor raster lines as the baseline. While the area measurement and the measured angles are thus completely arbitrary, the distribution of angles is real and experimentally relevant. These area and angle measurements were made for 500 replicates per micrograph, the area measurements discarded and angular measurements collated for frequency distribution. An artifact of the Bioquant software is that any ambiguous angular measurement is set equal to zero. If, for example, an area is defined by a quadrilateral, and two non-parallel sides are its longest dimensions, the reported angle will be zero. As a result, after filtering all zeros from the angular distribution sets, the number of valid measurements in different data sets was not equal. To compensate for this, the zeros were discarded and each data set was truncated at 400 measurements before sorting. This distribution was linearly transformed to a mean of 90 deg by determining the average of the raw distribution, and adding to or subtracting from all measurements a value such that the average of the new distribution was 90 deg. The new distribution was then examined to find the maximum and minimum values. From all values greater than 180 deg, 180 deg was subtracted, and 180 deg was added to all values less than 0 deg, to bring all data within the allowable range. This procedure allowed pooling of data from different micrographs at the same strain. Micrographs from both OsO_4 and glutaraldehyde-fixed samples were used.

The standard deviations of the angular measurement distributions, after truncation and rectification to 90 deg, were used to calculate a mean standard deviation for each strain. To quantify the vessel radial strain *vs.* distribution relationship, the plot of standard deviation *vs.* strain had a curve fitted to it by a variety of means and the fit that gave the highest correlation coefficient (r^2) was accepted.

Data analysis

An implicit assumption of the vessel stress calculations in the paper by McConnell *et al.* (1996) was the conservation of wall cross-sectional area. Briefly, it is assumed that, as the transmural pressure increased, the midwall radius of the vessel increased and the wall thickness decreased such that the area of a section through the vessel perpendicular to its axis was conserved:

$$A = \pi(r_o^2 - r_i^2)$$

$$A = \pi(r_o + r_i)(r_o - r_i)$$

$$A = \pi t(r_o + r_i) = \pi T(R_o + R_i). \quad (9)$$

Therefore $r_o + r_i = A/\pi t$ $R_o + R_i = A/\pi T$,

where T is wall thickness, r_o is the outer radius of the vessel, r_i is the inner radius, and A is the wall area (Davison *et al.* 1995). Note that capital letters denote resting values, taken to be in the zero-pressure state in this case. The strain acting on the vessel wall, then, was calculated for all vessels fixed in OsO_4 from:

$$\epsilon = \frac{r_{mw} - R_{mw}}{R_{mw}},$$

$$\epsilon = \frac{\left(\frac{r_o + r_i}{2}\right) - \left(\frac{R_o + R_i}{2}\right)}{\left(\frac{R_o + R_i}{2}\right)},$$

$$\epsilon = \frac{r_o + r_i - (R_o + R_i)}{R_o + R_i}, \quad (10)$$

$$\epsilon = \frac{r_o + r_i - (A/\pi T)}{A/\pi T}.$$

No zero-pressure (as opposed to zero-stress) samples were collected when the OsO_4-fixed vessel sections were prepared. In order to calculate the strain on the vessel wall, vessel sections of four animals were tested to determine any change in wall thickness between zero-pressure samples and zero-stress samples. Two narrow (2–5 mm) rings were cut from the abdominal aorta between the heart and the first lateral arteries. The wall of one of the rings was split to provide a zero-stress section, while the other was kept intact as a zero-pressure section. Samples were sectioned using a cryostat microtome at −20 °C, and wall thicknesses measured under a light microscope, with ocular micrometer, at ×100 magnification, ten times on each of five frozen slices through the wall perpendicular to the axis. Student's t test, assuming unequal variances, was performed to determine if the means differed, and their ratio taken to transform the osmium-fixed zero-stress thicknesses to zero-pressure thicknesses (t_o).

The model (Aspden, 1986) was programmed using the scripting language of Maple V (release 2, Waterloo Maple Software, Waterloo, Ontario, Canada). This software was also used to compute the model output. The program was tested against data estimated from the figures in the paper detailing the model and its behaviour. The integrals were evaluated using Simpson's rule, stepped over four intervals. This is the default number of intervals provided by Maple V (release 2), and was considered adequate for a first approximation.

The input strains, both circumferential and radial, were taken from data collected by Davison *et al.* (1995). Whole vessels were quasistatically inflated over about 25 s, each to a different strain, and allowed to deflate over the same period. Three data sets collected at different strain rates were chosen at random. Because the data was somewhat noisy, it was filtered by choosing every fifth point on the loading curve from its minimum to its maximum such that $n_{i+1} > n_i$. In the event that the fifth point did not satisfy this constraint, the next subsequent point which did satisfy it was chosen and the count resumed from that point. Correlation coefficients were calculated for predicted stress *versus* that observed by Davison *et al.* (1995), and tested for significant deviation from zero with a t test.

Note that all experimental uncertainties were propagated and reported as relative uncertainties unless otherwise noted.

RESULTS

Figure 3 shows the angular distribution measured from a vessel fixed in osmium tetroxide at zero stress, and Fig. 4 shows the distribution from a vessel fixed in osmium tetroxide at 2·64 kPa, both after linear transformation to a mean of 90 deg. The standard deviations of these distributions are 32·03 and 9·137 deg, respectively. The pooled, transformed standard deviations were plotted against circumferential strain (Fig. 5) and linear, polynomial, power, logarithmic and exponential regressions performed to determine the best fit. The logarithmic regression formula was chosen because it gave the highest correlation coefficient ($r^2 = 0{\cdot}721$) of all those used (linear, 0·287; polynomial (second order), 0·646; power, 0·518; and exponential, 0·296). The standard deviation of the angular distribution of the microfibrils was observed to be inversely proportional to strain such that:

$$S_\theta = -1{\cdot}9124 \ln(\epsilon) + 12{\cdot}26.$$

The mean wall thicknesses of zero-stress samples was $0{\cdot}125 \pm 0{\cdot}029$ mm, and differed significantly ($P < 0{\cdot}001$) from that of zero-pressure samples, which was $0{\cdot}178 \pm 0{\cdot}026$ mm. The mean ratio of zero-stress thicknesses to zero-pressure thicknesses was $1{\cdot}429 (\pm 0{\cdot}0387) : 1$. The volume fractions of microfibrils in artery walls did not differ by more than experimental uncertainty from a mean value of 0·282.

Figures 6, 7 and 8 compare the circumferential stresses predicted by Aspden's (1986) model with the corresponding data recorded by Davison *et al.* (1995). A correlation analysis of the calculated to the observed stresses was performed, and $r^2 = 0{\cdot}9952$ for Fig. 6, $r^2 = 0{\cdot}9956$ for Fig. 7 and $r^2 = 0{\cdot}9940$ for Fig. 8. All were significantly different from zero ($P < 0{\cdot}001$).

DISCUSSION

The correlations between the predictions from Aspden's (1986) model and the observations from Davison *et al.* (1995) (Figs 6, 7 and 8) are remarkable. The stress *vs.* strain curve for the vessel is completely characterized by the reorientation and deformation of microfibrils. In fact, it may be roughly partitioned into two phases. Examining Figs 5 and 6 (for example), early in the loading curve, up to a strain of about 0·60, microfibril reorientation plays the dominant role, much as the deformation of elastin does in mammalian arteries, or octopus artery elastomer in cephalopods (Gosline, 1980; Shadwick & Gosline, 1981; Shadwick & Gosline, 1985; Gosline, Shadwick, DeMont & Denny, 1988). At higher strains, greater than approximately 80%, where collagen begins to take the load in mammalian vessels, it is the deformation of the microfibrils that supports the circumferential stress. This may be a third evolutionary solution to the functional problem of compliant arteries needing to display non-linear elastic behaviour.

The evidence of evolutionary conservation of the fibrillin protein from medusans and sea cucumbers to humans (Reber-Müller *et al.* 1995; Thurmond, 1996; Thurmond & Trotter, 1996) implies that the mechanical properties of lobster microfibrils may apply generally to microfibrillar function in the animal kingdom. If that is the case, it indicates that the role played by microfibrils must extend well beyond their established function in elastic fibre development (Montes, 1992). The wide range of strains over which the microfibril-based tissues can remain operative (up to 3·0 in Fig. 8) may provide a means of load transfer to and from amorphous elastin in both statically loaded tissues, such as skin, and dynamically compliant tissues, such as arteries. The results presented here may then be used, with appropriate volume fraction measurements and distribution function estimates, to gain insight into microfibrillar function in other tissues and animals.

Few studies have been able to partition fully the contribution of fibre reorientation and/or deformation along the stress–strain curve of composite biomaterials. Indeed, this problem is generally very difficult to resolve, since *in situ* measurements of fibre deformation are difficult to make. The unique combination of fibres with 'built-in' markers for *in situ* strain measurements and the relatively simple architecture of the arterial wall used in this work have allowed us to make these measurements. We found that the change in angular distribution is inversely proportional to the increase in strain. This supports the idea that non-linear properties may be due, in part, to changes in the way embedded fibres are oriented, with respect to a stress vector, within a composite material. Essentially, the fraction of the load borne by an individual fibre, within a composite, is related to the angle that it makes with the stress vector. In general, the more closely a single fibre is aligned with the vector, the greater the load it must carry. The distribution of angles in the population of fibres, then, decreases as the load increases such that the stress is spread out over a sufficient number of individuals to bear it (Fig. 5).

The microfibrillar-based arterial systems found in primitive vertebrates and invertebrates (Davison *et al.* 1995) provide a unique model system to explore in considerable detail structure and function relationships of microfibrils, and will provide important information for the cure and prevention of connective tissue diseases such as Marfan syndrome. We are presently characterizing the microfibrils found in primitive vertebrates and invertebrates, and initiating work to correlate changes in the morphology of microfibrils with their mechancial function.

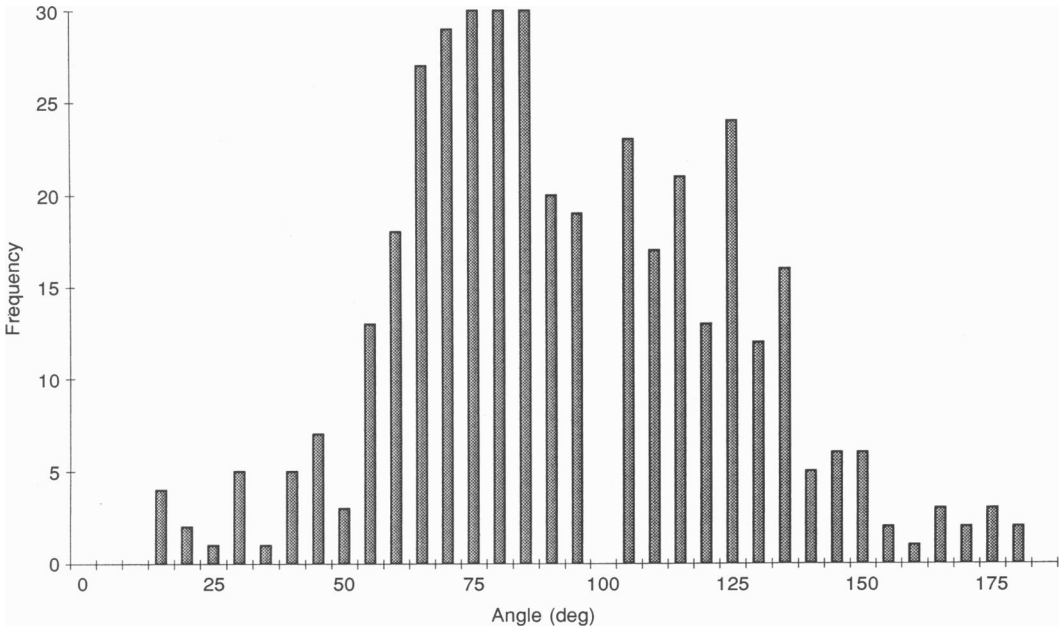

Figure 3

The angular distribution measured from a vessel fixed in osmium tetroxide at zero stress after linear transformation to a mean of 90 deg.

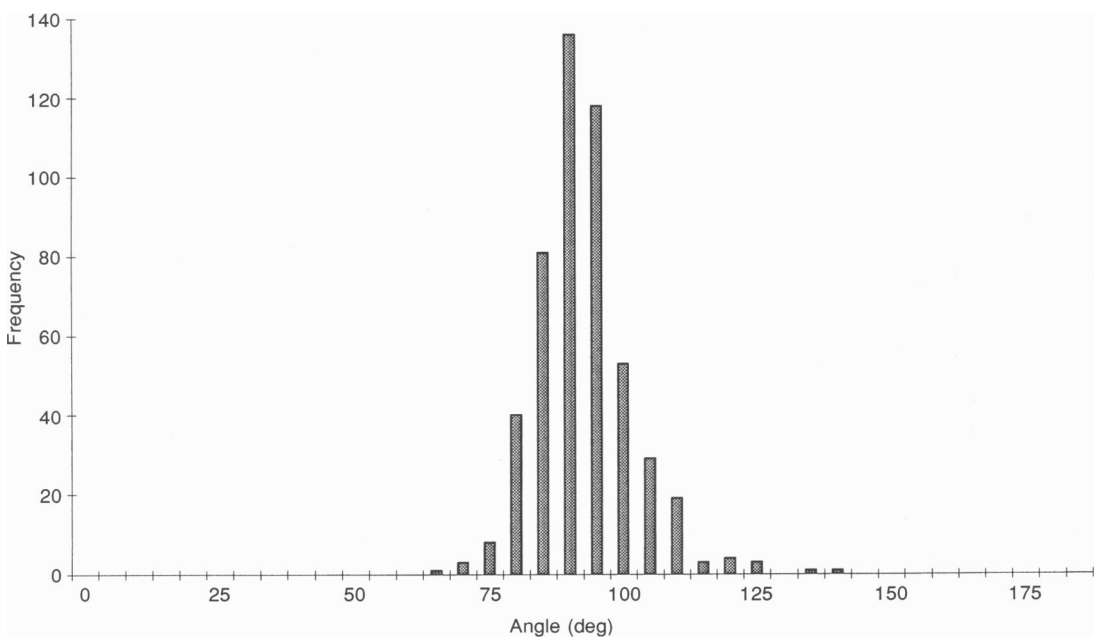

Figure 4

The angular distribution measured from a vessel fixed in osmium tetroxide at 2·64 kPa after linear transformation to a mean of 90 deg.

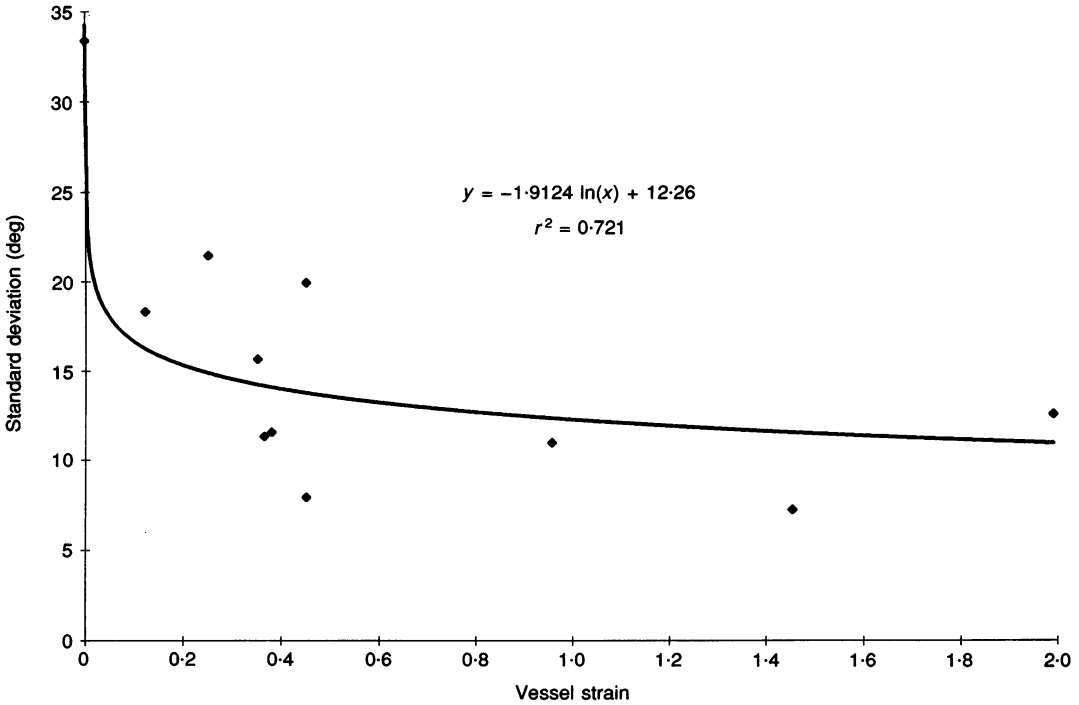

Figure 5

The standard deviation of the distribution of angles that microfibrils make with a radial line varies inversely with circumferential strain in the vessel wall.

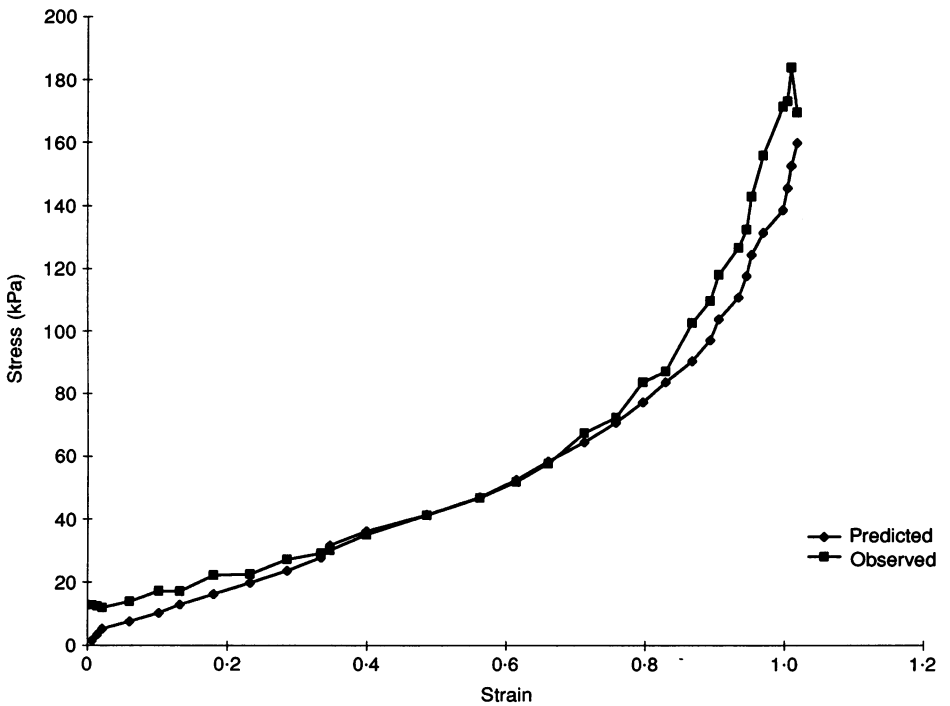

Figure 6

A comparison of predicted and observed stress for dataset no. 607 ($r^2 = 0{\cdot}995$) from Davison *et al.* (1995).

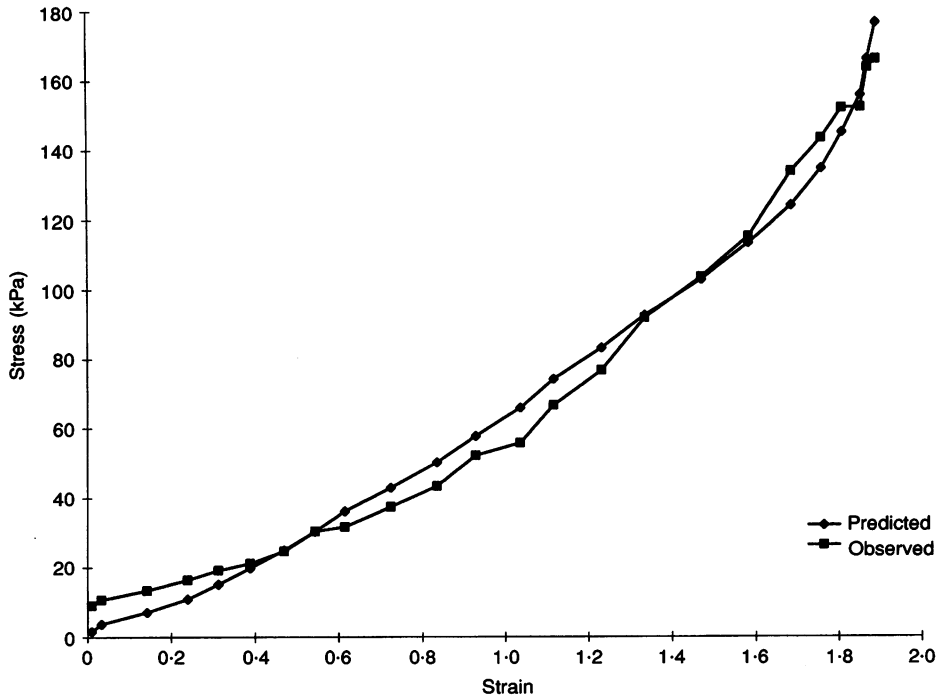

Figure 7
A comparison of predicted and observed stress for dataset no. 720 ($r^2 = 0{\cdot}996$) from Davison *et al.* (1995).

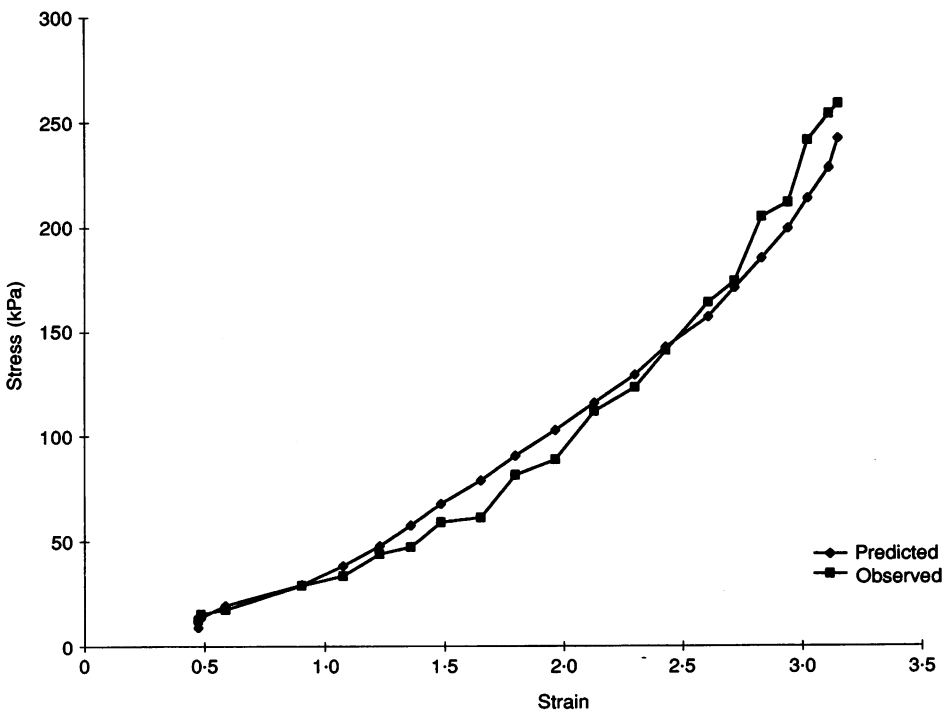

Figure 8
A comparison of predicted and observed stress for dataset no. 737 ($r^2 = 0{\cdot}994$) from Davison *et al.* (1995).

APPENDIX

Aspden's (1986) model calculates increments of stress, in a fibre-reinforced composite material, by multiplying together all of the factors that may influence the reinforcing fibres at each particular orientation relative to the stress vectors, and summing over all possible orientations:

$$\Delta\sigma_{ij} = \int_{-\pi/2}^{\pi/2} V_f E_f \Delta\epsilon_f g(\theta) l'_i l'_j \mathrm{d}\theta, \tag{A1}$$

where $\Delta\sigma_{ij}$ is an increment of stress, V_f is the volume fraction occupied by reinforcing fibres, E_f is their modulus of elasticity, $\Delta\epsilon_f$ is an increment of strain, $g(\theta)$ is a function of the angular distribution of these fibres, and l'_i and l'_j are direction cosines for a fibre relative to the stress vector.

Equation (A1), while concise, is not in an easily computable form. In the first place, since stress is a tensor, even though the off-diagonals are all zero, the equation represents not one but two integrals:

$$\Delta\sigma_{11} = \int_{-\pi/2}^{\pi/2} V_f E_f \Delta\epsilon_f g(\theta) l'_1 l'_1 \mathrm{d}\theta,$$

and:

$$\Delta\sigma_{22} = \int_{-\pi/2}^{\pi/2} V_f E_f \Delta\epsilon_f g(\theta) l'_2 l'_2 \mathrm{d}\theta. \tag{A1a}$$

Of these two, only the second is of interest to the investigation of the role played by microfibrils in the mechanical properties of the artery.

Let us assume the angular distribution is Gaussian. The standard deviation of the distribution was observed to vary inversely with strain, so it can comfortably be made a function of that quantity. The distribution function, $g(\theta)$ may then be stated:

$$g(\theta) = \frac{\exp\{[-(\theta_i - \bar{\theta})^2]/[2S^2(\epsilon)]\}}{S(\epsilon)\sqrt{2\pi}}, \tag{A2}$$

where θ_i is an individual angle of orientation, θ is the mean angle of orientation and $S(\epsilon)$ is the standard deviation of the distribution as a function of strain.

Clearly, the denominator of eqn (2) has no dependency on θ. Neither does the volume fraction of the fibres (V_f), nor does their modulus of elasticity (E_f). All of these quantities may be moved outside the integral, leaving equation (A1) as:

$$\Delta\sigma_{ij} = \frac{V_f E_f}{S(\epsilon)\sqrt{2\pi}} \int_0^{\pi} \Delta\epsilon_f \exp\{[-(\theta_i - \bar{\theta})^2]/[2S^2(\epsilon)]\} l'_i l'_j \mathrm{d}\theta. \tag{A3}$$

Next let us deal with the direction cosines, l'_i and l'_j. Aspden (1986) defines them in his eqn (2.8) as:

$$l'_i = \frac{l_i + \epsilon_{ij} l_i}{[1 + (\epsilon_{mn} l_m)^2 + 2\epsilon_{mn} l_m l_n]^{1/2}},$$

expanding for the case of l'_i:

$$l'_i = \frac{(1 + \epsilon_{11})l_1 + \epsilon_{12} l_2}{[1 + (\epsilon_{11} l_1 + \epsilon_{12} l_1 + \epsilon_{21} l_2 + \epsilon_{22} l_2)^2 + 2(\epsilon_{11} l_1^2 + \epsilon_{12} l_1 l_2 + \epsilon_{21} l_2 l_1 + \epsilon_{22} l_2^2)]^{1/2}}.$$

It is worth noting at this point that $\epsilon_{12} = \epsilon_{21} = 0$. Furthermore, as we are restricting ourselves to the two-dimensional case, any cross product between ϵ_{11} and ϵ_{22} has no meaning, and so is also set to zero. Continuing with the expansion, then:

$$l'_i = \frac{(1 + \epsilon_{11})l_1}{(1 + \epsilon_{11}^2 l_1^2 + \epsilon_{22}^2 l_2^2 + 2\epsilon_{11} l_1^2 + 2\epsilon_{22} l_2^2)^{1/2}}.$$

Now, $l_1 = \cos\theta$, $l_2 = \sin\theta$, and $l'_1 = \cos\theta'$, so:

$$l'_i = \cos\theta' = \frac{(1 + \epsilon_{11})\cos\theta}{(1 + \epsilon_{11}^2 \cos^2\theta + \epsilon_{22}^2 \sin^2\theta + 2\epsilon_{11}\cos^2\theta + 2\epsilon_{22}\sin^2\theta)^{1/2}}.$$

By Pythagoras:

$$1 = \cos^2\theta + \sin^2\theta.$$

So:

$$l_1' = \cos\theta' = \frac{(1+\epsilon_{11})\cos\theta}{(\cos^2\theta + \sin^2\theta + \epsilon_{11}{}^2\cos^2\theta + \epsilon_{22}{}^2\sin^2\theta + 2\epsilon_{11}\cos^2\theta + 2\epsilon_{22}\sin^2\theta)^{1/2}}.$$

Collecting like terms:

$$l_1' = \cos\theta' = \frac{(1+\epsilon_{11})\cos\theta}{(\epsilon_{11}{}^2\cos^2\theta + 2\epsilon_{11}\cos^2\theta + \cos^2\theta + \epsilon_{22}{}^2\sin^2\theta + 2\epsilon_{22}\sin^2\theta + \sin^2\theta)^{1/2}},$$

and factoring the denominator leaves:

$$l_1' = \cos\theta' = \frac{(1+\epsilon_{11})\cos\theta}{[(1+\epsilon_{11})^2\cos^2\theta + (1+\epsilon_{22})^2\sin^2\theta]^{1/2}}. \tag{A4}$$

By a similar argument:

$$l_2' = \sin\theta' = \frac{(1+\epsilon_{22})\sin\theta}{[(1+\epsilon_{11})^2\cos^2\theta + (1+\epsilon_{22})^2\sin^2\theta]^{1/2}}. \tag{A5}$$

The strain acting on the fibres is modified by these direction cosines according to Aspden's (1986) eqn (2.14):

$$\epsilon_f = \epsilon_{ij} l_j l_i' - (l_i' - l_i).$$

Expanding the summations and substituting from (A4) and (A5) yields:

$$\epsilon_f = \epsilon_{11}\cos\theta\cos\theta' + \epsilon_{12}\sin\theta\cos\theta' + \epsilon_{21}\cos\theta\sin\theta' + \epsilon_{22}\sin\theta\sin\theta' - \cos\theta'(\cos\theta' - \cos\theta) - \sin\theta'(\sin\theta' - \sin\theta).$$

Once again, all off diagonal components are zero, so:

$$\epsilon_f = \epsilon_{11}\cos\theta\cos\theta' + \epsilon_{22}\sin\theta\sin\theta' - \cos\theta^2 + \cos\theta'\cos\theta - \sin\theta^2 + \sin\theta'\sin\theta,$$

$$\epsilon_f = \epsilon_{11}\cos\theta\cos\theta' + \epsilon_{22}\sin\theta\sin\theta' - (\cos^2\theta' + \sin^2\theta') + \cos\theta'\cos\theta + \sin\theta'\sin\theta,$$

and

$$\epsilon_f = \epsilon_{11}\cos\theta\cos\theta' + \epsilon_{22}\sin\theta\sin\theta' + \cos(\theta' - \theta) - 1. \tag{A6}$$

Combining eqns (A3) and (A5) with (A1*a*):

$$\Delta\sigma_{22} = \frac{V_f E_f}{S(\epsilon)\sqrt{2\pi}} \int_0^{\pi} \frac{\Delta\epsilon_f \exp\{[-(\theta_i - \bar{\theta})^2]/[2S^2(\epsilon)]\}[(1+\epsilon_{22})\sin\theta']^2}{[(1+\epsilon_{11})^2\cos^2\theta + (1+\epsilon_{22})^2\sin^2\theta]} d\theta. \tag{A7}$$

It is at this point that this development deviates from Aspden's (1986) formulations. In his development of the many-fibre system, in order to preserve generality over systems that do not display linear deformation behaviour, his eqn (3.9) defines the true strain increment as:

$$\Delta\epsilon_f = \delta_n \prod_{i=1}^{n-1} (1 + \delta_i).$$

In such a non-linear system, the above product takes account of strain that may already be present in the tissue. Since the microfibrils have demonstrated linear deformation behaviour, each strain increment will deform those microfibrils parallel to a tangent to the vessel wall by the same amount as the last strain increment, or the next. There is no need to take account of any strain that may already be present in the tissue, except in the angular distribution function. That is, the deformation of the fibres is incremental, while the change in the angular distribution function is cumulative. This was accomplished by calculating:

$$\epsilon_1 = \Delta\epsilon_{11} = \epsilon_{11,n} - \epsilon_{11,n-1},$$

$$\epsilon_2 = \Delta\epsilon_{22} = \epsilon_{22,n} - \epsilon_{22,n-1},$$

for the purposes of eqn (A7), while feeding $\epsilon_{22,n}$ to the angular distribution function. Thus, eqn (A7) becomes, in expanded form:

$$\Delta\sigma_{22} = \frac{V_f E_f}{S(\epsilon)\sqrt{2\pi}}\left(\int_0^{\pi} \frac{\epsilon_1 \cos\theta \cos\theta' \exp\{[-(\theta_i - \bar{\theta})^2]/[2S^2(\epsilon)]\}\,[(1+\epsilon_2)\sin\theta]^2}{(1+\epsilon_1)^2\cos^2\theta + (1+\epsilon_2)^2\sin^2\theta}\,d\theta\right.$$

$$+\int_0^{\pi} \frac{\epsilon_2 \sin\theta \sin\theta' \exp\{[-(\theta_i - \bar{\theta})^2]/[2S^2(\epsilon)]\}\,[(1+\epsilon_2)\sin\theta]^2}{(1+\epsilon_1)^2\cos^2\theta + (1+\epsilon_2)^2\sin^2\theta}\,d\theta$$

$$+\int_0^{\pi} \frac{\cos\theta \cos\theta' \exp\{[-(\theta_i - \bar{\theta})^2]/[2S^2(\epsilon)]\}\,[(1+\epsilon_2)\sin\theta]^2}{(1+\epsilon_1)^2\cos^2\theta + (1+\epsilon_2)^2\sin^2\theta}\,d\theta$$

$$-\int_0^{\pi} \frac{\sin\theta \sin\theta' \exp\{[-(\theta_i - \bar{\theta})^2]/[2S^2(\epsilon)]\}\,[(1+\epsilon_2)\sin\theta]^2}{(1+\epsilon_1)^2\cos^2\theta + (1+\epsilon_2)^2\sin^2\theta}\,d\theta$$

$$\left.-\int_0^{\pi} \frac{\exp\{[-(\theta_i - \bar{\theta})^2]/[2S^2(\epsilon)]\}\,[(1+\epsilon_2)\sin\theta]^2}{(1+\epsilon_1)^2\cos^2\theta + (1+\epsilon_2)^2\sin^2\theta}\,d\theta\right).$$

Substituting for $\cos\theta'$ and $\sin\theta'$ gives:

$$\Delta\sigma_{22} = \frac{V_f E_f}{S(\epsilon)\sqrt{2\pi}}\left(\int_0^{\pi} \frac{\epsilon_1(1+\epsilon_1)(1+\epsilon_2)^2\sin^2\theta\cos^2\theta \exp\{[-(\theta_i - \bar{\theta})^2]/[2S^2(\epsilon)]\}}{[(1+\epsilon_1)^2\cos^2\theta + (1+\epsilon_2)^2\sin^2\theta]^{3/2}}\,d\theta\right.$$

$$+\int_0^{\pi} \frac{\epsilon_2(1+\epsilon_2)^3\sin^4\theta \exp\{[-(\theta_i - \bar{\theta})^2]/[2S^2(\epsilon)]\}}{[(1+\epsilon_1)^2\cos^2\theta + (1+\epsilon_2)^2\sin^2\theta]^{3/2}}\,d\theta$$

$$+\int_0^{\pi} \frac{(1+\epsilon_1)(1+\epsilon_2)^2\sin^2\theta\cos^2\theta \exp\{[-(\theta_i - \bar{\theta})^2]/[2S^2(\epsilon)]\}}{[(1+\epsilon_1)^2\cos^2\theta + (1+\epsilon_2)^2\sin^2\theta]^{3/2}}\,d\theta$$

$$+\int_0^{\pi} \frac{(1+\epsilon_2)^3\sin^4\theta \exp\{[-(\theta_i - \bar{\theta})^2]/[2S^2(\epsilon)]\}}{[(1+\epsilon_1)^2\cos^2\theta + (1+\epsilon_2)^2\sin^2\theta]^{3/2}}\,d\theta$$

$$\left.+\int_0^{\pi} \frac{(1+\epsilon_2)^2\sin^2\theta \exp\{[-(\theta_i - \bar{\theta})^2]/[2S^2(\epsilon)]\}}{(1+\epsilon_1)^2\cos^2\theta + (1+\epsilon_2)^2\sin^2\theta}\,d\theta\right). \quad \text{(A8)}$$

The final items of consideration in this development are the limits of integration. Certainly, it is valid to integrate the above equation over the maximum allowable range of angles. It is not, however, necessary to do so. The entire purpose of this model is to account for the reorientation of supporting members, microfibrils in this case, as the material as a whole comes under strain. It follows, then, that only the contribution of those members that are sufficiently aligned with the stress vector for that increment being calculated to play a significant role should be included in that stress increment. A member that is nearly perpendicular to the stress vector is not going to make a significant contribution to the increment. It is shown by Aspden's (1986) eqn (2.14) that only members lying in the range of angles $0 \leqslant \theta \leqslant \theta_{max}$ play a role in supporting tension, where (adapted to the two dimensional case from Aspden's (1986) eqn (4.1)):

$$\theta_{max} = \left(\frac{1-(1+\epsilon_{11})^2}{(1+\epsilon_{22})^2 - (1+\epsilon_{11})^2}\right)^{1/2}.$$

So eqn (A8) becomes:

$$\Delta\sigma_{22} = \frac{V_f E_f}{S(\epsilon)\sqrt{2\pi}}\left(\int_0^{\theta_{max}} \frac{\epsilon_1(1+\epsilon_1)(1+\epsilon_2)^2\sin^2\theta\cos^2\theta\exp\{[-(\theta_i-\bar{\theta})^2]/[2S^2(\epsilon)]\}}{[(1+\epsilon_1)^2\cos^2\theta+(1+\epsilon_2)^2\sin^2\theta]^{3/2}}d\theta\right.$$

$$+\int_0^{\theta_{max}} \frac{\epsilon_2(1+\epsilon_2)^3\sin^4\theta\exp\{[-(\theta_i-\bar{\theta})^2]/[2S^2(\epsilon)]\}}{[(1+\epsilon_1)^2\cos^2\theta+(1+\epsilon_2)^2\sin^2\theta]^{3/2}}d\theta$$

$$+\int_0^{\theta_{max}} \frac{(1+\epsilon_1)(1+\epsilon_2)^2\sin^2\theta\cos^2\theta\exp\{[-(\theta_i-\bar{\theta})^2]/[2S^2(\epsilon)]\}}{[(1+\epsilon_1)^2\cos^2\theta+(1+\epsilon_2)^2\sin^2\theta]^{3/2}}d\theta$$

$$+\int_0^{\theta_{max}} \frac{(1+\epsilon_2)^3\sin^4\theta\exp\{[-(\theta_i-\bar{\theta})^2]/[2S^2(\epsilon)]\}}{[(1+\epsilon_1)^2\cos^2\theta+(1+\epsilon_2)^2\sin^2\theta]^{3/2}}d\theta$$

$$\left.+\int_0^{\theta_{max}} \frac{(1+\epsilon_2)^2\sin^2\theta\exp\{[-(\theta_i-\bar{\theta})^2]/[2S^2(\epsilon)]\}}{(1+\epsilon_1)^2\cos^2\theta+(1+\epsilon_2)^2\sin^2\theta}d\theta\right),$$

which is eqn (8).

AARON, B. B. & GOSLINE, J. M. (1981). Elastin as a random-network elastomer: a mechanical and optical analysis of single elastin fibers. *Biopolymers* **20**, 1247–1260.

ASPDEN, R. M. (1986). Relation between structure and mechanical behaviour of fibre-reinforced composite materials at large strains. *Proceedings of the Royal Society* A **406**, 287–298.

AULT, H. K. & HOFFMAN, A. H. (1992*a*). A composite micromechanical model for connective tissues: part I – theory. *Journal of Biomechanical Engineering* **114**, 137–141.

AULT, H. K. & HOFFMAN, A. H. (1992*b*). A composite micromechanical model for connective tissues: part II – application to rat tail tendon and joint capsule. *Journal of Biomechanical Engineering* **114**, 142–146.

BERGEL, D. H. (1961). The dynamic elastic properties of the arterial wall. *Journal of Physiology* **156**, 458–469.

DAVISON, I. G., WRIGHT, G. M. & DEMONT, M. E. (1995). The structure and physical properties of invertebrate and primitive vertebrate arteries. *Journal of Experimental Biology* **198**, 2185–2196.

DEMONT, M. E. & GOSLINE, J. M. (1988). Mechanics of jet propulsion in the hydromedusan jellyfish, *Polyorchis penicillatus* I. Mechanical properties of the locomotor structure. *Journal of Experimental Biology* **134**, 313–332.

GODFREY, M., MENACHE, V. & WELEBER, R. G. (1990). Cosegregation of elastic-associated microfibrillar abnormalities with the Marfan phenotype in families. *American Journal of Human Genetics* **46**, 652–663.

GODFREY, M., MICHAEL, R. & STEINMANN, B. (1995). Abnormal morphology of fibrillin microfibrils in fibroblast cultures from patients with neonatal Marfan Syndrome. *American Journal of Pathology* **146**, 1414–1424.

GOSLINE, J. M. (1980). The elastic properties of rubber-like proteins and highly extensible tissues. In *Society for Experimental Biology Symposium XXXIV, The Mechanical Properties of Biological Materials*, ed. VINCENT, J. F. V. & CURREY, J. D., pp. 331–357. Society for Experimental Biology, London.

GOSLINE, J. M., SHADWICK, R. E., DEMONT, M. E. & DENNY, M. W. (1988). Non-gaussian elastic properties in biopolymer networks. In *Biological and Synthetic Polymer Networks*, ed. KRAMER, D., pp. 57–77. Elsevier Applied Science, London.

HOLLISTER, D. W., GODFREY, M. & SAKAI, L. Y. (1994). Immunohistologic abnormalities of the microfibrillar-fibre system in the Marfan Syndrome. *New England Journal of Medicine* **323**, 152–165.

HUDETZ, A. G. (1979). Incremental elastic modulus for orthoptic incompressible arteries. *Journal of Biomechanics* **12**, 651–655.

KEENE, D. R., MADDOX, K., KUO, H., SAKAI, L. Y. & GLANVILLE, R. W. (1991). Extraction of extendable beaded structures and their identification as fibrillin-containing extracellular matrix microfibrils. *Journal of Histochemistry and Cytochemistry* **39**, 441–449.

KIELTY, C. M., CUMMINGS, C., WHITTAKER, S. P., SHUTTLEWORTH, C. A. & GRANT, M. E. (1991). Isolation and ultrastructural analysis of microfibrillar structures from foetal bovine elastic tissues. *Journal of Cell Science* **99**, 797–807.

MCCONNELL, C. J., WRIGHT, G. M. & DEMONT, M. E. (1996). The modulus of elasticity of lobster aorta microfibrils. *Experientia* **52**, 918–921.

MALAK, T. W. & BELL, S. C. (1994). Distribution of fibrillin-containing microfibrils and elastin in human fetal membranes: a novel molecular basis for membrane elasticity. *American Journal of Obstetrics and Gynecology* **171**, 195–203.

MECHAM, R. P. & HEUSER, J. E. (1991). The elastic fiber. In *Cell Biology of Extracellular Matrix*, 2nd edn, ed. HAY, E. D., pp. 79–109. Plenum Press, New York.

MONTES, G. S. (1992). Distribution of oxytalan, elaunin and elastic fibres in tissues. *Journal of the Brazilian Association for the Advancement of Science* **44**, 224–233.

RAMIREZ, F., PEREIRA, L., ZHANG, H. & LEE, B. (1993). The fibrillin–Marfan syndrome connection. *BioEssays* **15**, 589–594.

Reber-Müller, S., Spissinger, T., Schuchert, P., Spring, J. & Schmid, V. (1995). An extracellular matrix protein of jellyfish homologous to mammalian fibrillins forms different fibrils depending on the life stage of the animal. *Developmental Biology* **169**, 662–672.

Reinhart, D. P., Keene, D. R., Corson, G. M., Poschl, E., Bacjinger, H. P., Gambee, J. E. & Sakai, L. Y. (1996). Fibrillin-1: Organization in microfibrils and structural properties. *Journal of Molecular Biology* **258**, 104–116.

Sakai, L. Y., Keene, D. R. & Engvall, E. (1986). Fibrillin, a new 350-kd glycoprotein, is a component of extracellular microfibrils. *Journal of Cell Biology* **103**, 2499–2509.

Shadwick, R. E. (1992). Circulatory structure and mechanics. In *Biomechanics – Structures and Systems*, ed. Biewener, A. A., pp. 233–261. Oxford University Press, Toronto.

Shadwick, R. E. & Gosline, J. M. (1981). Elastic arteries in invertebrates: mechanics of the octopus aorta. *Science* **213**, 759–761.

Shadwick, R. E. & Gosline, J. M. (1985). Mechanical properties of the octopus aorta. *Journal of Experimental Biology* **114**, 259–284.

Thurmond, F. A. (1996). Characterization of collagen fibrils and the fibrillin microfibrillar network of echinoderm mutable collagenous tissues. PhD Thesis, Univeristy of New Mexico, Albuquerque, NM, USA.

Thurmond, F. A. & Trotter, J. A. (1996). Morphology and biomechanics of the microfibrillar network of sea cucumber dermis. *Journal of Experimental Biology* **199**, 1817–1828.

Weibel, E. R. (1979). *Stereological Methods*, vol. I. Academic Press, New York.

Acknowledgements

This work was funded by a NIH (US) Grant to M.E.D. and NSERC (Canada) Grants to M.E.D. and G.M.W. We thank J. Cheng (Biology, St Francis Xavier University), J. Quinn (Mathematics, St Francis Xavier University) and D. Wadowska (University of Prince Edward Island) for their excellent assistance.

Author's email address

M. E. DeMont: edemont@stfx.ca

Received 27 June 1996; accepted 4 November 1996.